

# Fluorene-based oligomers as red light-emitting materials: a density functional theory study

Xue-Feng Ren · Ai-Min Ren · Lu-Yi Zou ·  
Ji-Kang Feng

Received: 29 November 2009 / Accepted: 25 February 2010 / Published online: 13 March 2010  
© Springer-Verlag 2010

**Abstract** The electronic structures, charge injection and transport, absorption and emission spectra, properties of two series of fluorene-based oligomers {2-[2-{2-[5-(9H-Fluoren-3-yl)-thiophen-2-yl]-vinyl}-6-(2-thiophen-2-yl-vinyl)-pyran-4-ylidene]-malononitrile}<sub>n</sub> (FTPM)<sub>n</sub> and {2-{2-[5-(9H-Fluoren-2-yl)-2-hydroxy-3-methoxy-phenyl]-vinyl}-6-[2-(2-hydroxy-3-methoxy-phenyl)-vinyl]-pyran-4-ylidene}-malononitrile}<sub>n</sub> (FOOPM)<sub>n</sub> ( $n = 1\text{--}4$ ) have been investigated by the density functional theory (DFT) approach. The ground-state geometries of (FTPM)<sub>4</sub> and (FOOPM)<sub>4</sub> optimized at B3LYP/6-31G(d) level exhibited zigzag arrangements. The energies of HOMO and LUMO, HOMO–LUMO energy gaps ( $\Delta E_{H-L}$ ) of (FTPM)<sub>n</sub> and (FOOPM)<sub>n</sub> ( $n = \infty$ ) were obtained by linear extrapolation method. Moreover, the calculations of ionization potential (IP), electronic affinity (EA), and reorganization energy ( $\lambda$ ) were used to evaluate the charge injection and transport abilities. For (FTPM)<sub>4</sub> and (FOOPM)<sub>4</sub>, the TDDFT calculations revealed that the absorption peaks can be characterized as  $\pi\text{--}\pi^*$  transition and couple with the location of electron density distribution changes in different repeat units. All the earlier theoretical investigations are intended to establish the structure–property relationships, which can provide guidance to design the organic light-emitting diodes (OLEDs) with high performance.

---

**Electronic supplementary material** The online version of this article (doi:[10.1007/s00214-010-0740-8](https://doi.org/10.1007/s00214-010-0740-8)) contains supplementary material, which is available to authorized users.

---

X.-F. Ren · A.-M. Ren (✉) · L.-Y. Zou · J.-K. Feng  
State Key Laboratory of Theoretical and Computational  
Chemistry, Institute of Theoretical Chemistry, Jilin University,  
130023 Changchun, People's Republic of China  
e-mail: aimin.ren@gmail.com

**Keywords** Oligomers · DFT · Organic light-emitting diodes (OLEDs)

## 1 Introduction

Remarkable improvements have been observed in the development of organic light-emitting diodes (OLEDs) by using polymers materials [1–3]. To obtain three primary RGB (red, green, and blue) colors [4–7], many polymers including poly(p-phenylene)s, poly(phenylenevinylene)s, poly[2,7-(9,9-dialkylfluorene)]s, poly(oxadiazole)s, poly(3,6-carbazole)s, poly(2,7-carbazole)s, and poly(3,9-carbazole)s have been synthesized in the past decade. Among these polymers, polyfluorene derivatives (PFs) are the most promising light-emitting materials because of their interesting and unique chemical and physical properties, such as high fluorescence efficiency and good thermal stability [8–10].

Nonetheless, one of major problems in the application of polymer light-emitting diodes (PLEDs) is unbalanced carrier injection and transport, especially for PFs. Many attempts have been made to modulate the highest occupied molecular orbital (HOMO) and low-lying lowest unoccupied molecular orbital (LUMO) energies, ionization potential (IP), and electron affinity (EA) by controlling conjugation length and introducing the electron-donating or electron-accepting substitutions in PFs [11–14]. Recently, a series of PFs containing 2-pyran-4-ylidene-malononitrile (PM) unit were synthesized [15], which displayed decreased LUMO and improved EA. To rationalize these attractive photophysical properties, our group explored the electronic structures and photophysical properties of poly{(2,7-fluorene)-alt-(2-{2,6-bi-[2-(4-phenylene)vinyl]pyran-4-ylidene}-malononitrile)} (FPM)<sub>n</sub> [16]

( $n = 1\text{--}4$ ) and poly{(2,7-fluorene)-alt-(2-{2,6-bi-[2-(2-methoxy-5-phenylene)vinyl]pyran-4-ylidene}-malononitrile)} ( $\text{FOPM}_n$ ) [16] ( $n = 1\text{--}4$ ) by theoretical studies. The calculated results showed that  $(\text{FPM})_n$  had improved electron-injection ability. Moreover, it had improved the charge-carrier transport rate and charge transfer balance performance, indicating that  $(\text{FPM})_n$  had potential applications in field of OLEDs as single-layer electroluminescent material.

More recently, Chen et al. [17] have synthesized and reported the electrochemical and photophysical properties of this type of copolymer poly{2-[2-{2-[5-(9H-Fluoren-3-yl)-thiophen-2-yl]-vinyl}-6-(2-thiophen-2-yl-vinyl)-pyran-4-ylidene]-malononitrile}, and poly{2-{2-[2-[5-(9H-Fluoren-2-yl)-2-hydroxy-3-methoxy-phenyl]-vinyl}-6-[2-(2-hydroxy-3-methoxy-phenyl)-vinyl]-pyran-4-ylidene]-malononitrile}, namely  $(\text{FTPm})_n$  and  $(\text{FOOPM})_n$ , respectively. These copolymers can function as solar cells, due to their broad optical absorption, low band gaps, and possibly high mobility. Additionally, they have the advantage of low-lying LUMO energy, about  $-3.54$  eV. Herein, we further explore the ground-state geometries, electronic spectra, and low-lying excited state of  $(\text{FTPm})_n$  and  $(\text{FOOPM})_n$  ( $n = 1\text{--}4$ ) by using density functional theory (DFT), time-dependent DFT (TDDFT), and singlet configuration interaction (CIS) methods to find out if these oligomers are potential emitting materials for OLEDs. To learn more about the roles played by the thiophene and 2-methoxyphenol groups, we compare the energies of HOMO and LUMO, HOMO–LUMO energy gaps ( $\Delta E_{H-L}$ ) of  $(\text{FTPm})_n$  and  $(\text{FOOPM})_n$  ( $n = 1\text{--}4$ ) with those of  $(\text{FPM})_n$  [16],  $(\text{FOPM})_n$  [16], and PF [18]. Particularly, the variations of IP, EA, reorganization energy ( $\lambda$ ) of  $(\text{FTPm})_n$  are calculated to investigate the charge injection and transport.

## 2 Computational methods

The ground-state structures of oligomers  $(\text{FTPm})_n$  ( $n = 1\text{--}4$ ) were fully optimized by B3LYP [19, 20]/6-31G(d), B3PW91 [21, 22]/6-31G(d), and BH&HLYP [23]/6-31G(d), respectively. Based on earlier calculated results and available experimental values (HOMO and LUMO energies) (detailed discussions of exchange and correlation (XC) modeling for oligomers are in the supporting information.), it is found the B3LYP/6-31G(d) is suitable for this type of oligomer. In viewing this, the ground-state structures as well as their ions structures of oligomers  $(\text{FOOPM})_n$  ( $n = 1\text{--}4$ ) and the ionic structures of  $(\text{FTPm})_n$  ( $n = 1\text{--}4$ ) were fully optimized by B3LYP/6-31G(d). Furthermore, various photophysical properties of these complexes, including ionization potential (IP), electron affinity (EA), and reorganization energy ( $\lambda$ ) of  $(\text{FTPm})_n$

( $n = 1\text{--}4$ ) were calculated on the basis of optimized structures. Then, all the earlier photophysical properties of polymers  $(\text{FTPm})_n$  were obtained through a linear extrapolation, which had been successfully employed to investigate several series of polymers [24–26]. The transition energies of  $(\text{FTPm})_n$  and  $(\text{FOOPM})_n$  ( $n = 1\text{--}4$ ) will be calculated using TD-DFT//B3LYP/6-31g(d) calculation.

Considering huge computational cost for large molecules, the lowest singlet excited-state ( $S_1$ ) geometries of  $(\text{FTPm})_n$  and  $(\text{FOOPM})_n$  ( $n = 1\text{--}3$ ) were optimized by singlet configuration interaction (CIS) [27] with 3-21G(d) basis sets. And the emission spectra of them were obtained by TD-B3LYP/3-21G(d) at the excited-states structures. All these calculations were performed on the SGI origin 2000 server, using Gaussian 03 program package [28].

## 3 Results and discussion

### 3.1 Grounds-state geometries

The labeled schemes of  $(\text{FTPm})_n$  and  $(\text{FOOPM})_n$  are depicted in Fig. 1. For monomer FTPM and FOOPM, both cis- and trans-isomeric forms are optimized at the B3LYP/6-31G(d) level, as illustrated in Fig. 2. The calculated energy of trans-FTPm is merely lower by 0.011 kcal/mol than that of cis-FTPm, and the energy of trans-FOOPM is only lower 0.021 kcal/mol than that of cis-FOOPM. Obviously, the energy differences between cis- and trans-isomers of both FTPM and FOOPM are very small. Then, taking FTPM as an example, we optimized isomers of dimer and trimer. The optimized structures and relative energies of these isomers are drawn in Fig. S1 in supporting information. The photophysical properties for these isomer, such as the HOMO and LUMO energies, IP(v), and EA(v),

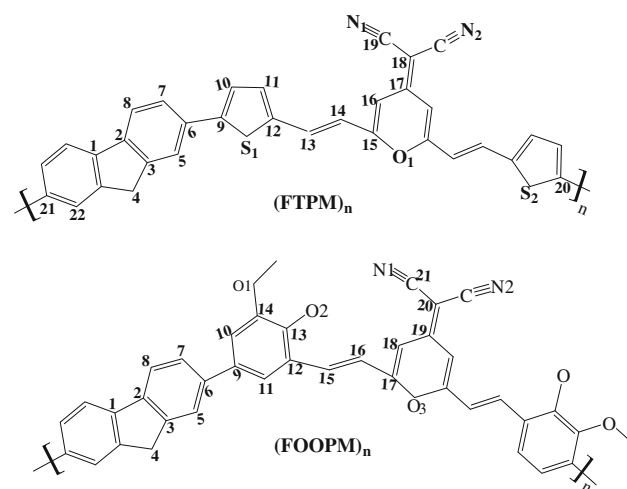


**Fig. 1** The sketch map of the  $(\text{FTPm})_n$  and  $(\text{FOOPM})_n$

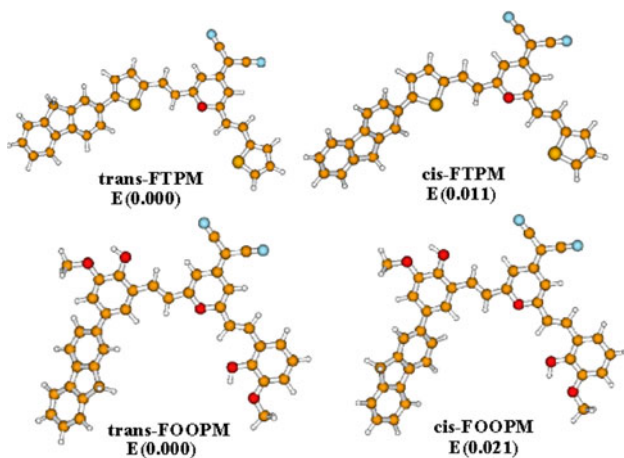


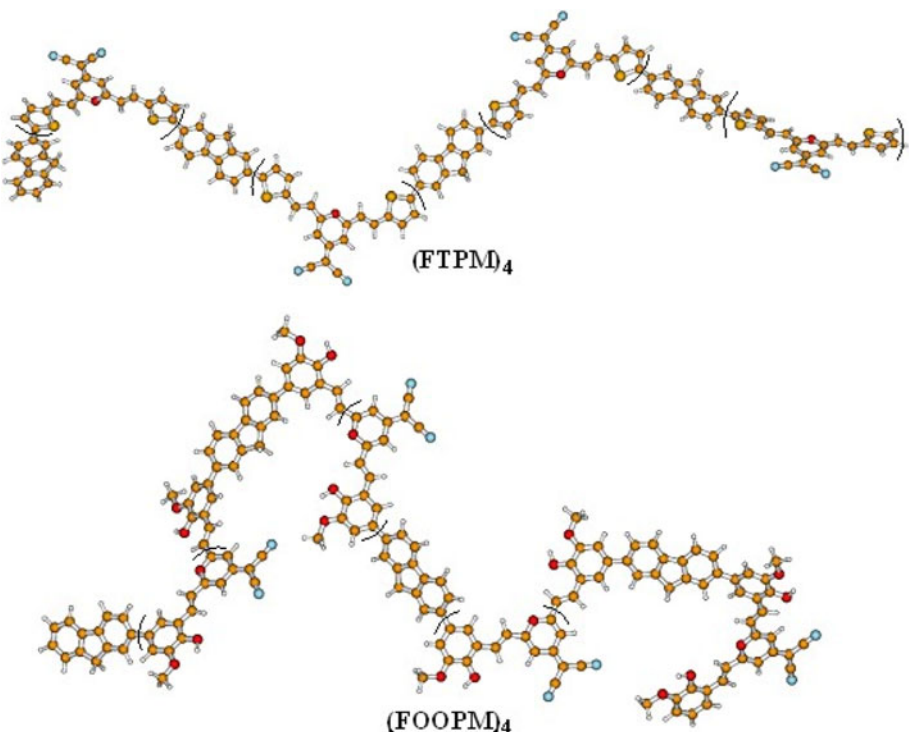
**Fig. 2** The trans- and cis-structures and relative energies (in kcal/mol) of monomer FTPM and FOOPM at the B3LYP/6-31G(d) level

are listed in Table S2 in supporting information. Based on these investigations, it is found that photophysical properties for these isomers are similar with each other, indicating that the isomers will not affect the following prediction for photophysical properties of these oligomers. Therefore, to save the computation resources, we will take one of the optimized geometries of the isomers to discuss.

Figure 3 shows the optimized geometries of  $(\text{FTPM})_4$  and  $(\text{FOOPM})_4$ . The selected bond lengths, bond angles, and dipole moments of  $(\text{FTPM})_n$  and  $(\text{FOOPM})_n$  ( $n = 1\text{--}4$ ) calculated by DFT are listed in Table 1 (see Supporting Information Table S3 for more geometry structures). As

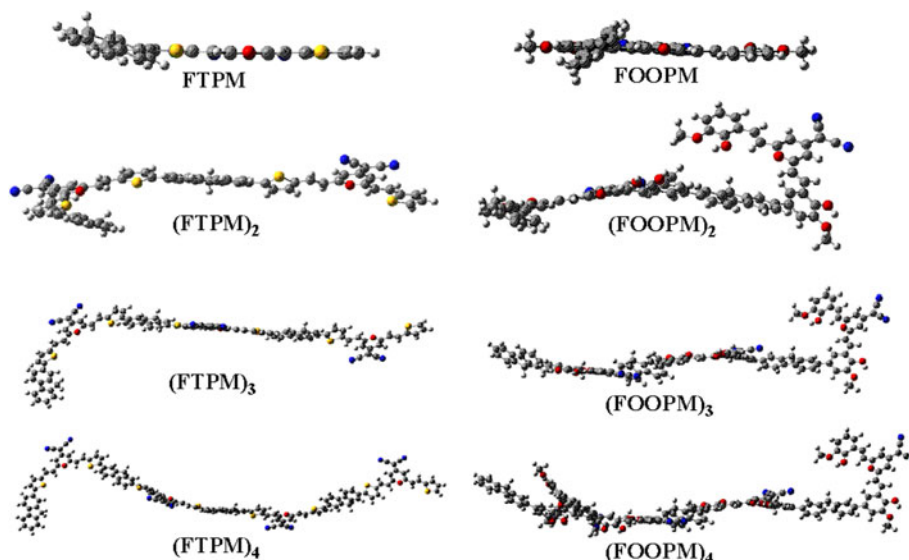
drawn in Fig. 3,  $(\text{FTPM})_4$  displays zigzag arrangement. Table 1 shows the inter-ring angle  $S_2\text{--}C_{20}\text{--}C_{21}\text{--}C_{22}$  on each monomer is about  $165^\circ$ . Obviously, the whole molecule is not coplanar. Due to this kind of arrangement, the steric effect between the repeat units can be reduced and therefore result in stabilized molecule structures. The stable conformation of  $(\text{FOOPM})_4$  represents zigzag arrangement too. Furthermore, the 2-{2,6-bis-[2-(5-methyl-thiophen-2-yl)-vinyl]-pyran-4-ylidene}-malononitrile segment on each monomer for  $(\text{FTPM})_n$  ( $n = 1\text{--}4$ ) tends to keep near planar conformation, as drawn in bracket in Fig. 3. Obviously, for  $(\text{FOOPM})_4$ , the planar part (as the 2-{2-[2-(2-Hydroxy-3-methoxy-phenyl)-vinyl]-6-methyl-pyran-4-ylidene}- malononitrile segment) on each monomer, becomes smaller than that of  $(\text{FTPM})_4$ . The side view of optimized structures of  $(\text{FTPM})_n$  and  $(\text{FOOPM})_n$  ( $n = 1\text{--}4$ ) is drawn in Fig. 4. As depicted in Fig. 4, the FTPM has relatively better plane geometry structure than FOOPM. It indicates that the  $\pi$ -conjugation interaction of FTPM is better than FOOPM. With the repeat unit increasing, the whole coplanar structures of both  $(\text{FTPM})_n$  and  $(\text{FOOPM})_n$  ( $n = 2\text{--}4$ ) are getting worse. However, considering the local planar segment on each repeat unit in  $(\text{FTPM})_4$  is larger than that of  $(\text{FOOPM})_4$ , as drawn in Fig. 3. Therefore, we infer that the  $\pi$ -conjugated interaction of  $(\text{FTPM})_n$  is better than  $(\text{FOOPM})_n$ . In addition, as listed in Table 1, FTPM has smaller dipole moment than that of FOOPM. For both  $(\text{FTPM})_n$  and  $(\text{FOOPM})_n$ , with increasing the repeat units, their dipole moments become

**Fig. 3** Optimized structures of the oligomers  $(\text{FTPM})_4$  and  $(\text{FOOPM})_4$ , the planar conformation on each monomer is drawn in bracket



**Table 1** Selected bond lengths ( $\text{\AA}$ ) and bond angles ( $^\circ$ ) of the optimized  $(\text{FTPM})_n$  and  $(\text{FOOPM})_n$  ( $n = 1\text{--}4$ ) by B3LYP/6-31G(d) method

$(\text{FTPM})_n$				$(\text{FOOPM})_n$			
$n = 1$	$n = 2$	$n = 3$	$n = 4$	$n = 1$	$n = 2$	$n = 3$	$n = 4$
<i>Bond length</i> ( $\text{\AA}$ )							
C <sub>6</sub> –C <sub>9</sub>	1.463	1.463	1.463	C <sub>6</sub> –C <sub>9</sub>	1.485	1.485	1.485
C <sub>12</sub> –C <sub>13</sub>	1.435	1.438	1.438	C <sub>12</sub> –C <sub>15</sub>	1.458	1.459	1.459
<i>Bond angle</i> ( $^\circ$ )							
C <sub>7</sub> –C <sub>6</sub> –C <sub>9</sub>	121.39	120.57	120.84	C <sub>7</sub> –C <sub>6</sub> –C <sub>9</sub>	120.78	120.97	120.91
S <sub>1</sub> –C <sub>12</sub> –C <sub>13</sub>	124.62	121.75	121.02	C <sub>11</sub> –C <sub>12</sub> –C <sub>15</sub>	123.81	123.40	123.44
C <sub>13</sub> –C <sub>14</sub> –C <sub>15</sub>	125.26	125.28	125.32	C <sub>15</sub> –C <sub>16</sub> –C <sub>17</sub>	125.10	125.41	125.43
<i>Dihedral angles</i> ( $^\circ$ )							
C <sub>7</sub> –C <sub>6</sub> –C <sub>9</sub> –S <sub>1</sub>	−25.61			C <sub>7</sub> –C <sub>6</sub> –C <sub>9</sub> –C <sub>11</sub>	39.20		
S <sub>2</sub> –C <sub>20</sub> –C <sub>21</sub> –C <sub>22</sub>		155.92	156.11	165.49			
<i>Dipole moment</i> ( $D$ )							
	11.67	8.22	13.18	18.08		13.05	26.51
						37.75	50.73

**Fig. 4** The side view of optimized structures of  $(\text{FTPM})_n$  and  $(\text{FOOPM})_n$  ( $n = 1\text{--}4$ )

large. And  $(\text{FOOPM})_4$  has the largest dipole moment. All of these results indicate that there may be a relationship between  $\pi$ -conjugated interaction and dipole moment for two series in the study, that is, poor  $\pi$ -conjugation interaction results in large dipole moment.

By comparing the bond lengths of  $(\text{FTPM})_n$  and  $(\text{FOOPM})_n$  ( $n = 1\text{--}4$ ), it is found that the bond lengths in fluorene and 2-pyran-4-ylidenemalononitrile (PM) fragments have small changes with different conjugated adjacent units. Actually, the main structural changes happen between the adjacent units of each monomer. For example, the inter-ring bond lengths C<sub>6</sub>–C<sub>9</sub> and C<sub>12</sub>–C<sub>13</sub> of  $(\text{FTPM})_4$  are 1.464 and 1.439  $\text{\AA}$ , respectively, nevertheless inter-ring bond lengths C<sub>6</sub>–C<sub>9</sub> and C<sub>12</sub>–C<sub>15</sub> of  $(\text{FOOPM})_4$  are 1.485 and 1.459  $\text{\AA}$ , respectively. In addition, the DFT-calculated bond lengths and bond angles of  $(\text{FTPM})_n$  ( $n = 1\text{--}4$ ) have

small changes with increasing the repeated units, the same as  $(\text{FOOPM})_n$  ( $n = 1\text{--}4$ ). As shown in Table 1, the bond lengths and bond angles deviations are less than 0.002  $\text{\AA}$  and 2°, respectively. It suggests that the basic structures of the polymers can be described as their oligomers.

### 3.2 Frontier molecular orbitals

The HOMO and LUMO energies obtained by DFT//B3LYP/6-31g(d) of polymers  $(\text{FTPM})_n$  and  $(\text{FOOPM})_n$  are obtained through a linear extrapolation and drawn in Fig. 5. The contour plots of HOMOs and LUMOs for  $(\text{FTPM})_4$  and  $(\text{FOOPM})_4$  (see Fig. S2 in supporting information for smaller oligomers) are shown in Fig. 6. And detailed frontier molecular orbital energies, as well as the HOMO–LUMO energy gaps ( $\Delta E_{H-L}$ ) of  $(\text{FTPM})_n$  and

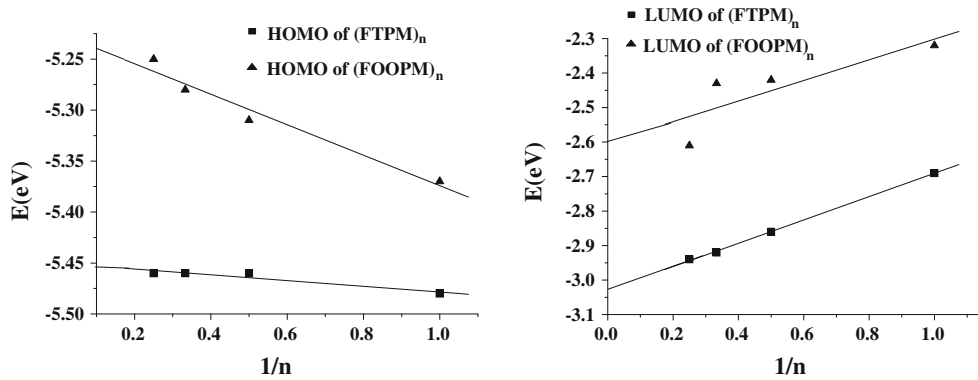
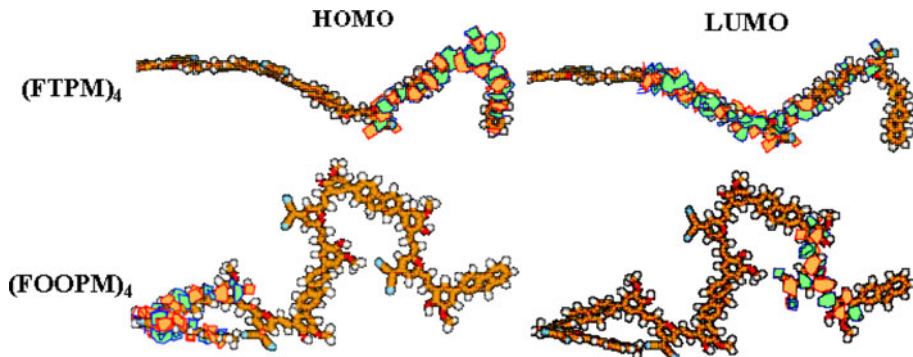


**Fig. 5** The HOMO and LUMO energies (in eV) of  $(FTPM)_n$  and  $(FOOPM)_n$  as a function of the reciprocal number of the repeated units  $n$  in oligomers

**Fig. 6** Plots of the HOMOs and LUMOs for  $(FTPM)_4$  and  $(FOOPM)_4$



$(FOOPM)_n$  ( $n = 1\text{--}4$ ) are listed in Table S4 in supporting information, together with the available experimental results. [17]

Figure 5 shows that the LUMO energies of  $(FTPM)_n$  and  $(FOOPM)_n$  decrease with increasing chain length. Compared with referenced compounds  $(FPM)_n$  [16], the LUMO energy ( $-3.03$  eV) in  $(FTPM)_n$  is small, suggesting that the replacement of benzene by thiophene unit in  $(FPM)_n$  has improved the electron-injection ability. Nevertheless, the LUMO energy ( $-2.60$  eV) in  $(FOOPM)_n$  is larger than  $(FOPM)_n$  ( $-2.82$  eV) [16], which implies that the introduction of 2-methoxyphenol in  $(FOPM)_n$  has decreased the ability of electronic injection. In addition, the HOMO energy of  $(FTPM)_n$  ( $-5.46$  eV) is higher than that of  $(FPM)_n$  ( $-5.66$  eV) [16], while the HOMO energy of  $(FOOPM)_n$  ( $-5.24$  eV) is higher than that of  $(FOPM)_n$  ( $-5.41$  eV) [16], indicating that thiophene and 2-methoxyphenol units play roles in enhancing the hole-injection abilities. As shown in Fig. 5 and Table S4, there are some deviations between the theoretical calculations and experiment results [17]. Actually, in experiment, the HOMO and LUMO energies are estimated from an empirical formula proposed by Brédas et al. [29], which are based on the onset of the oxidation and reduction peaks measured by cyclic voltammetry [29], whereas, theoretical

calculations do not consider the polarization effects and intermolecular packing forces. Therefore, the deviations between the calculations and experiment results are unavoidable.

Figure 5 and Table S4 also show that the calculated  $\Delta E_{H-L}$  of  $(FTPM)_n$  and  $(FOOPM)_n$  is gradually narrowed with increasing repeated units. It means that promoting an electron from HOMO to LUMO becomes easier as  $n$  growing. And the  $\Delta E_{H-L}$  of  $(FTPM)_n$  ( $2.43$  eV) is smaller than that of  $(FOOPM)_n$  ( $2.64$  eV), suggesting that the larger  $\pi$ -conjugated extent can lower the  $\Delta E_{H-L}$ . Furthermore, the  $\Delta E_{H-L}$  of  $(FTPM)_n$  and  $(FOOPM)_n$  is smaller than referenced compounds  $(FPM)_n$  [16],  $(FOPM)_n$  [16], and PF [18]; therefore,  $(FTPM)_n$  and  $(FOOPM)_n$  are easier to promote the electron from HOMO to LUMO than referenced compounds. Obviously, the  $\Delta E_{H-L}$  can be adjusted by the introduction of thiophene and 2-methoxyphenol into polymers. Consequently, we believe that  $(FTPM)_n$  and  $(FOOPM)_n$  will have more favorable optical properties than referenced compounds.

As illustrated in Fig. S2, for monomer FTPM, the HOMO mainly spreads over the PM and fluorene, but the LUMO is located on PM and thiophene. Apparently, the fluorene unit is functionalized as electron donor, and the thiophene is used as electron acceptor. With

increasing the repeat unit, HOMOs and LUMOs of  $(\text{FTPM})_n$  and  $(\text{FOOPM})_n$  ( $n = 2\text{--}4$ ) display local  $\pi$  characteristics. Take  $(\text{FOOPM})_4$  as an example, the HOMO is mainly located on the one unit, while LUMO is mostly distributed on the next unit. Clarke et al. [30] suggested that the analyses of spatial distribution of molecular orbitals are useful to understand the promotion of an electron from HOMO to LUMO. It is argued that, little orbital overlap between HOMO and LUMO implies a less intense transition from HOMO to LUMO [31]. As drawn in Fig. 6 and Fig. S2, the degree of electron density overlapping between HOMO and LUMO for  $(\text{FTPM})_n$  and  $(\text{FOOPM})_n$  becomes low with increasing the repeating units. It implies that the HOMO–LUMO transition would have small contribution to the main optical transition, which will be further testified in Sect. 3.4. In addition, it is noteworthy that PM unit plays an important role in all the HOMOs and LUMOs of  $(\text{FTPM})_n$  and  $(\text{FOOPM})_n$  ( $n = 1\text{--}4$ ). They are consistent with referenced compounds [16]  $(\text{FPM})_n$  and  $(\text{FOPM})_n$  ( $n = 1\text{--}4$ ).

### 3.3 Charge injection and transfer

As well known, the performance of OLEDs depends on the adequate and balanced charge injection and transfer. The ionization potential (IP) and electron affinity (EA) have been successfully used to estimate the energy barrier for the holes and electrons into the polymer, respectively [16, 18, 26]. In general, the lower IP value of the hole-transport layer (HTL), the easier the entrance of holes from ITO to HTL; and the higher EA value of the electron-transport layer (ETL), the easier the entrance of electrons from cathode to ETL.

Considering  $(\text{FTPM})_n$  has lower LUMO energy and smaller  $\Delta E_{H-L}$  than those of  $(\text{FOOPM})_n$ ,  $(\text{FPM})_n$ , [16], and  $(\text{FOPM})_n$  [16], we take  $(\text{FTPM})_n$  as an example to investigate the charge injection and transport in this section. The IP and EA can be calculated by both vertical excitations (v, at the geometry of the neutral molecule) and adiabatic excitations (a, optimized structure for both the neutral and

charged molecule). The hole extraction potential (HEP) and electron extraction potential (EEP) are the energy differences between cation/anion and neutral molecules at their optimized geometries. The DFT-calculated IP, EA, and extraction potential (EP) of  $(\text{FTPM})_n$  ( $n = 1\text{--}4$ ) are listed in Table S5 in supporting information. Through the extrapolation, [24–26] these properties of polymers are drawn in Fig. 7. As revealed in Fig. 7, the IP(v)s, IP(a)s, and HEP of  $(\text{FTPM})_n$  progressively decrease, while their EA(v)s, EA(a)s, and EEP gradually increase as  $n$  increase from 1 to 4. And the IP(v) (5.74 eV) of  $(\text{FTPM})_n$  is smaller than referenced compounds  $(\text{FPM})_n$  and  $(\text{FOPM})_n$ . This clearly indicates that the presence of thiophene units benefit the hole-injection ability. It is consistent with the conclusion HOMO energy analysis in Sect. 3.2. The EA(v) of  $(\text{FTPM})_n$  (2.74 eV) is larger than that of  $(\text{FPM})_n$  [16], suggesting that it is a potential electron-injection material.

According to the Marcus electron-transfer theory [32], the charge-transfer rate can be described as the formula (1)

$$K = \left( \frac{\pi}{\lambda K_b T} \right)^{\frac{1}{2}} \times \frac{V^2}{h} \times \exp\left( -\frac{\lambda}{4K_b T} \right) \quad (1)$$

where  $T$  is the temperature,  $K_b$  is the Boltzmann constant, and  $\lambda$  is the reorganization energy due to geometric relaxation accompanying charge transfer. And  $V$  is the electronic coupling matrix element, which lies on the center distance between the donator and acceptor normally. Apparently, the  $V$  appears to be important element for determining the transfer rate; however, intramolecular charge-transfer range in noncrystal is very narrow and its magnitude is very limited [33, 34], therefore the motilities of electrons and holes are expected to be dominated by the internal reorganization energies ( $\lambda$ ). As illustrated in formula (1), to achieve a high electron-transfer rate, the  $\lambda$  needs to be small. The  $\lambda$  can be calculated as our groups have reported [16, 26]:

$$\lambda_{\text{hole}} = \text{IP}(v) - \text{HEP} \quad (2)$$

$$\lambda_{\text{electron}} = \text{EEP} - \text{EA}(v) \quad (3)$$

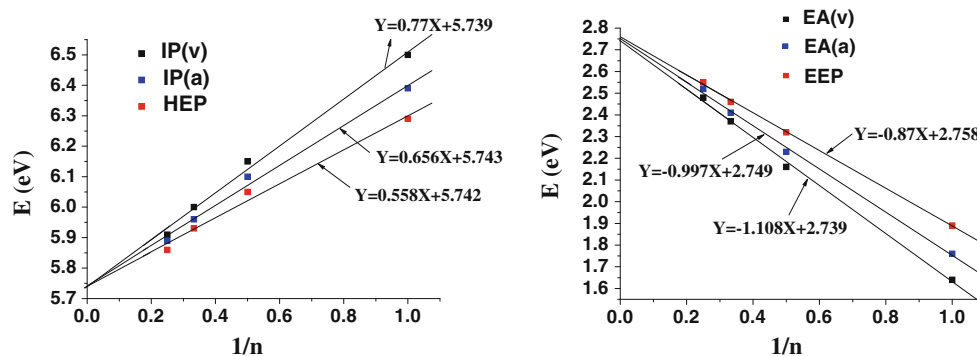


**Fig. 7** IP(v), IP(a), HEP, EA(a), EA(v), and EEP of the  $(\text{FTPM})_n$  as a function of the reciprocal number of the repeated units  $n$  in oligomers

**Table 2** Calculated hole and electron reorganization energies for  $(\text{FTPm})_n$ 

$(\text{FTPm})_n$	$n = 1$	$n = 2$	$n = 3$	$n = 4$	$n = \infty$
$\lambda_{\text{hole}}$	0.21	0.10	0.07	0.05	0.00
$\lambda_{\text{electron}}$	0.25	0.16	0.09	0.07	0.02

(unit in eV)

The DFT-calculated  $\lambda_{\text{hole}}$  and  $\lambda_{\text{electron}}$  of  $(\text{FTPm})_n$  ( $n = 1\text{--}4$ ) are listed in Table 2. As listed in Table 2, the  $\lambda_{\text{hole}}$  and  $\lambda_{\text{electron}}$  values for  $(\text{FTPm})_n$  decrease with the repeating unit numbers increase, suggesting that the hole and electron-transfer rates would increase as  $n$  increasing. Whereas the  $\lambda_{\text{hole}}$  values for  $(\text{FTPm})_n$  (0.0 eV) are much smaller than that of  $(\text{FPM})_n$  (0.06 eV) [16]. This shows that the incorporation of thiophene unit has improved the hole-transfer rate. As expected,  $(\text{FTPm})_n$  has improved charge-injection ability and hole-transport rate, so it is a potential emitting material in OLEDs.

### 3.4 UV-vis absorption spectra

On the basis of the optimized ground-state geometry, vertical excitation energy (eV), oscillator strength, and main configurations are calculated by the TD B3LYP/6-31G(d) methods. Based on the earlier calculated results, simulated electronic absorption spectra of studied compounds are shown in Fig. 8. The density contour plots of the transition orbitals for the main absorption bands of  $(\text{FTPm})_4$  and  $(\text{FOOPM})_4$  are drawn in Figs. 9 and 10, respectively. The detailed UV-vis absorption wavelength, oscillator strength, and main configurations are listed in Table S6 in supporting information.

Table S6 shows that the lowest optically allowed electronic transition  $S_0 \rightarrow S_1$  at 483.68, 528.45, 540.88, 545.81 nm for  $(\text{FTPm})_n$  as  $n$  increase from 1 to 4, respectively, has the largest oscillator strengths ( $f$ ). Furthermore, the electronic transition  $S_0 \rightarrow S_1$  is gradually red-shifted and oscillator strength increases from FTPM to  $(\text{FTPm})_4$ , which is apparently caused by the gradual increased  $\pi$ -conjugation chain length. As shown in Table S6, the contribution of HOMO-LUMO transition to  $S_1$  decreases with repeated unit increase, which are consistent with the analysis of the electron density distribution of HOMO and LUMO in Sect. 3.2. Furthermore, as listed in Table S4, the energy differences between HOMO-1 and HOMO in  $(\text{FTPm})_2$  (0.07 eV), HOMO-2/HOMO-1 and HOMO in  $(\text{FTPm})_3$  (0.09/0.06 eV), HOMO-3/HOMO-2 and HOMO in  $(\text{FTPm})_4$  (0.10/0.08 eV) are very small. Therefore, the electron transition from these inner occupied orbitals to LUMO or LUMO +1 is comparable to that from HOMO to LUMO.

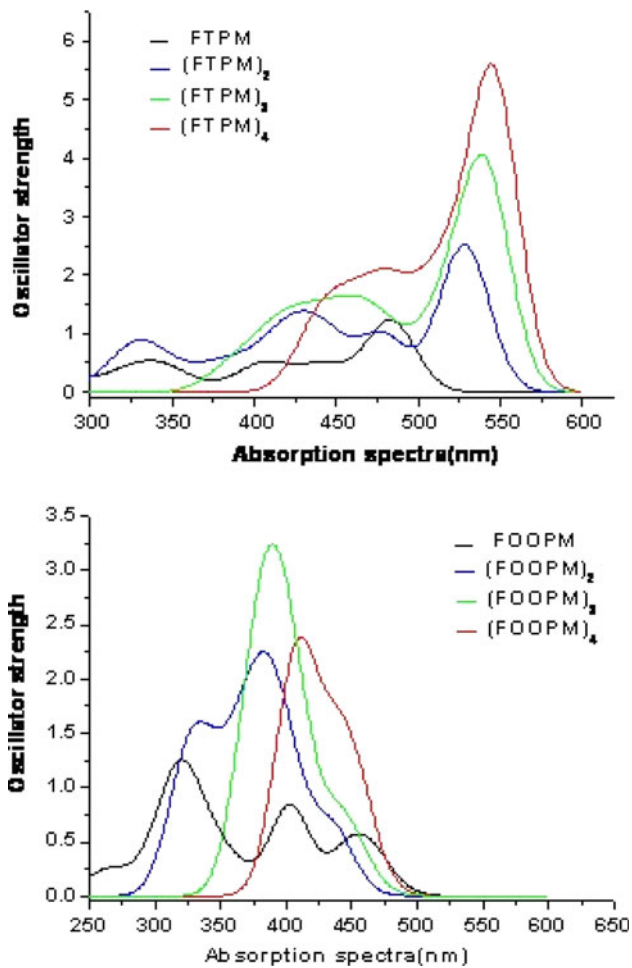


**Fig. 8** The simulated Gaussian type absorption spectra of  $(\text{FTPm})_n$  and  $(\text{FOOPM})_n$  ( $n = 1\text{--}4$ ) obtained by TDDFT//B3LYP/6-31G(d) method

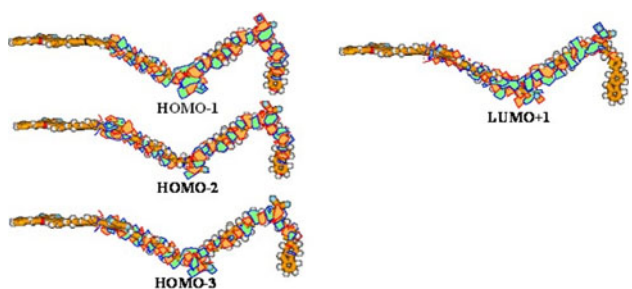
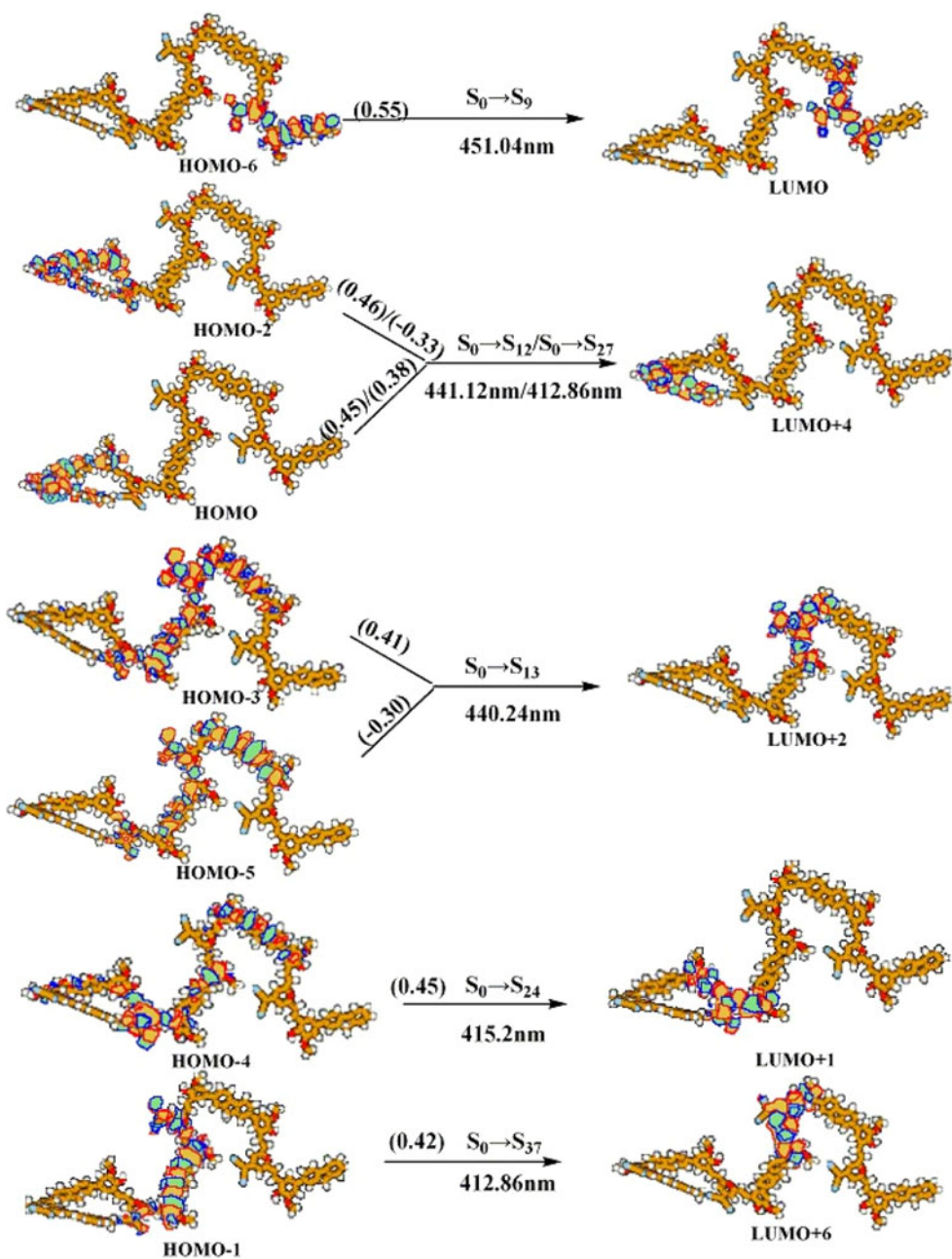


**Fig. 9** The density diagram plots for the transition orbitals of  $S_1$ ,  $S_3$ , and  $S_4$  absorptions of  $(\text{FTPm})_4$

In addition,  $(\text{FTPm})_4$  is taken as an example to analyze the electronic transition. As illustrated in Figs. 6 and 9, the HOMO-3 and HOMO-2 of  $(\text{FTPm})_4$  are  $\pi$  orbital characteristic, which are mainly located on the first and second unit, whereas the LUMO and LUMO +1 mainly localize on these parts and display  $\pi^*$  characteristics. Therefore, the lowest-lying absorption at 545.81 nm of  $(\text{FTPm})_4$ , which is

**Fig. 10** The density diagram plots of the  $S_9$ ,  $S_{12}$ ,  $S_{13}$ ,  $S_{24}$ ,  $S_{27}$ , and  $S_{37}$  absorptions of  $(FOOPM)_4$  with main CI coefficient as drawn in bracket



contributed by the excitations of  $HOMO-3 \rightarrow LUMO$  ( $CI = 0.45$ ) and  $HOMO-2 \rightarrow LUMO + 1$  ( $CI = 0.29$ ), is assigned to  $\pi-\pi^*$  type transitions. The electronic excited states of  $S_3$  and  $S_4$ , (515.77 and 513.14 nm) correspond to the promotion of an electron from the  $HOMO-1$  to  $LUMO$  and from  $HOMO$  to  $LUMO$  or  $LUMO + 1$ , which are assigned as transitions of  $\pi-\pi^*$  type and the location of electron density distribution from the first unit to the second unit. In addition, for  $(FOOPM)_4$ , as shown in Fig. 10, the electron transitions comprised the  $S_9$ ,  $S_{12}$ , and  $S_{13}$  are characterized as  $\pi-\pi^*$  type transition, while the location of electron density distribution change from the third unit to the second unit. Similarly, Fig. 10 shows that the electron

transitions comprised the  $S_{24}$ ,  $S_{27}$ , and  $S_{37}$  are also assigned to the  $\pi-\pi^*$  type transition, while the location of electron density distribution change in different repeat units.

### 3.5 The excited-state geometries and fluorescence spectra

Fluorescence spectrum means the lowest vibrational state of the excited electronic state drops down to one of the various vibrational levels of the ground electronic state, emitting a photon in the process. Since the calculation of excited-state geometries ( $S_1$ ) requires significantly computational cost, we only optimized the  $(FTPM)_n$  and

**Fig. 11** The side view of optimized  $S_1$  of  $(\text{FTPM})_n$  and  $(\text{FOOPM})_n$  ( $n = 1-3$ )

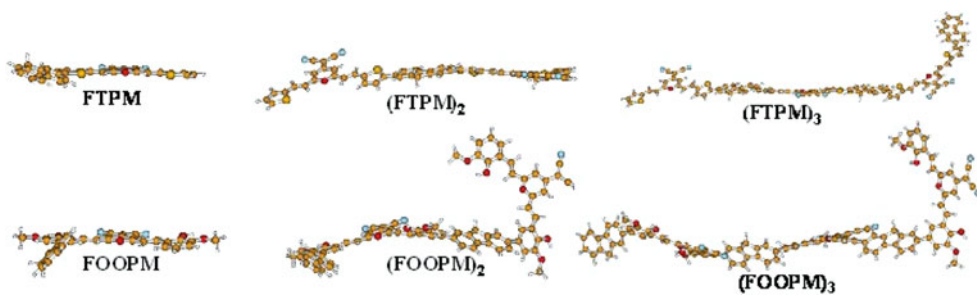


**Table 3** Emission spectra obtained by TDDFT/B3LYP/3-21G\* for  $(\text{FTPM})_n$  and  $(\text{FOOPM})_n$  ( $n = 1-3$ )

	Electronic transitions	$E_{\text{Flu}}$ (eV)	$E_b$ (eV)	Wavelengths (nm)	$f$	MO/character	Coefficient
FTPM	$S_1 \rightarrow S_0$	2.34	0.45	530.41	1.0115	HOMO $\rightarrow$ LUMO	0.59
$(\text{FTPM})_2$	$S_1 \rightarrow S_0$	2.25	0.35	551.34	1.6467	HOMO $\rightarrow$ LUMO	0.61
$(\text{FTPM})_3$	$S_1 \rightarrow S_0$	2.26	0.28	549.68	2.1128	HOMO $\rightarrow$ LUMO	0.61
FOOPM	$S_1 \rightarrow S_0$	2.51	0.54	494.47	0.2811	HOMO $\rightarrow$ LUMO	0.57
$(\text{FOOPM})_2$	$S_1 \rightarrow S_0$	2.53	0.36	489.41	0.3278	HOMO $\rightarrow$ LUMO	0.57
$(\text{FOOPM})_3$	$S_1 \rightarrow S_0$	2.52	0.33	492.40	0.3284	HOMO $\rightarrow$ LUMO	0.58

$(\text{FOOPM})_n$  ( $n = 1-3$ ) by CIS/3-21G(d) method. And the side view of optimized  $S_1$  of  $(\text{FTPM})_n$  and  $(\text{FOOPM})_n$  ( $n = 1-3$ ) is drawn in Fig. 11. The emission spectra of  $(\text{FTPM})_n$  and  $(\text{FOOPM})_n$  ( $n = 1-3$ ) obtained by TDDFT/B3LYP/3-21G(d) are listed in Table 3.

Table 3 shows that the calculated emission spectrum at 551.34 nm for  $(\text{FTPM})_2$  exhibits a red-shifted trend from that of FTPM (530.41 nm), which is consistent with the elongation of the conjugated chain, as drawn in Fig. 11. However, the third unit in  $(\text{FTPM})_3$  is not in a plane. Similarly, it is observed that the second and third unit in  $(\text{FOOPM})_2$  and  $(\text{FOOPM})_3$  are not in a plane, respectively. Consequently, the emission spectra of  $(\text{FTPM})_3$  and  $(\text{FOOPM})_n$  ( $n = 2, 3$ ) are not linear red-shifted by increasing the number of units, as listed in Table 3.

In addition, based on our group previous report [35], the exciton binding energy ( $E_b$ ), which indicates the energy required to destroy a hole-electron exciton, should be another important factor responsible for fluorescence efficiency. It can be computed by the following formula (in eV).

$$E_b = \Delta E_{H-L} - E_{\text{Flu}} \quad (4)$$

where  $E_{\text{Flu}}$  is the excitation energy. Accordingly, the  $E_b$  values of  $(\text{FTPM})_n$  and  $(\text{FOOPM})_n$  ( $n = 1-3$ ) are computed and listed in Table 3. As listed in Table 3, the  $E_b$  values for  $(\text{FOOPM})_n$  and  $(\text{FTPM})_n$  ( $n = 1-3$ ) decrease with the repeating unit numbers increase. Furthermore, the  $E_b$  values of  $(\text{FTPM})_3$  (0.28 eV) are smaller than that of  $(\text{FOOPM})_3$  (0.33 eV), indicating that  $(\text{FTPM})_3$  is easier to destroy the hole-electron excitations than  $(\text{FOOPM})_3$ .

#### 4 Conclusion

In this study, we have systematically investigated a series of copolymers containing fluorene and 2-pyran-4-ylidene-malononitrile (PM) units. Comparing with the referenced compounds  $(\text{FPM})_n$  and  $(\text{FOPM})_n$ , it is found that the introduction of thiophene and 2-methoxyphenol in this type of copolymers has lowered the LUMO energy, lifted the HOMO energies, and narrowed HOMO–LUMO gaps. This indicates that the electronic structure and photophysical properties can be adjusted by the introduction of thiophene and 2-methoxyphenol into polymers. Furthermore,  $(\text{FTPM})_n$  has decreased IP, increased EA, and decreased  $\lambda_{\text{hole}}$  values, suggesting that  $(\text{FTPM})_n$  is an excellent charge injection and transportation material. And the  $E_b$  value of  $(\text{FTPM})_3$  is smaller than that of  $(\text{FOOPM})_3$ , indicating that  $(\text{FTPM})_3$  is easier to destroy the hole-electron excitations than  $(\text{FOOPM})_3$ . The electronic spectra results reveal that the former peak of  $(\text{FTPM})_4$  (the lowest-lying absorption at 545.81 nm) is assigned to  $\pi-\pi^*$  type transition, while the latter absorption peaks [the electronic excited states of  $S_3$  (515.77 nm) and  $S_4$  (513.14 nm)] can be characterized as combination of  $\pi-\pi^*$  type transition and location of electron density distribution from the first unit to the second unit. All the earlier calculated results show that  $(\text{FTPM})_n$  is a potential red-emitting material in OLEDs.

**Acknowledgments** This work is supported by the Major State Basis Research Development Program (No. 2002CB 613406) and the National Natural Science Foundation of China (No. 20673045 and 20973078), and the Open Project of State Key Laboratory of

Supramolecular Structure and Materials of Jilin University (No. SKLSSM200716).

## References

- Wong KT, Chien YY, Chen RT, Wang CF, Lin YT, Chiang HH, Hsieh PY, Wu CC, Chou CH, Su YO, Lee GH, Peng SM (2002) *J Am Chem Soc* 124:11576
- Hancock JM, Gifford AP, Zhu Y, Lou Y, Jenekhe SA (2006) *Chem Mater* 18:4924
- Kim JH, Lee H (2002) *Chem Mater* 14:2270
- Grem G, Paar C, Stampfl J, Leising G (1995) *Chem Mater* 7:2
- Brown AR, Bradley DDC, Burroughes JH, Friend RH, Greenham NC, Burn PL, Holmes AB, Kraft A (1992) *Appl Phys Lett* 61:2793
- Vestweber H, Greiner A, Lemmer U, Mahrt RF, Richert R, Heitz W, Bässler H (1992) *Adv Mater* 4:661
- Pei Q, Yang Y (1996) *J Am Chem Soc* 118:7416
- Grell M, Bradley DDC, Inbasekaran M, Woo EP (1997) *Adv Mater* 9:798
- Redecker M, Bradley DDC, Inbasekaran M, Woo EP (1998) *Appl Phys Lett* 73:1565
- Janietz S, Bradley DDC, Grell M, Giebel C, Inbasekaran M, Woo EP (1998) *Appl Phys Lett* 73:2453
- Beaupré S, Leclerc M (2002) *Adv Funct Mater* 12:192
- Lévesque L, Donat-bouillud A, Tao Y, D'Iorio M, Beaupré S, Blondin P, Ranger M, Bouchard J, Leclerc M (2001) *Synth Met* 122:79
- Lee JI, Klaerner G, Davey MH, Miller RD (1999) *Synth Met* 102:1087
- Charas A, Barbagallo N, Morgado J, Alcacer L (2001) *Synth Met* 122:2
- Peng Q, Lu ZY, Huang Y, Xie M-G, Han S-H, Peng J-B, Cao Y (2004) *Macromolecules* 37:260
- Ren XF, Bo DS, Ren AM, Feng JK, Du LP, Sun CC (2009) *J Mol Struct (THEOCHEM)* 904:91
- Chen H, Cai XR, Xu ZG, Zhang T, Song B, Li Y, Jiang Q, Xie MG (2008) *Polym Bulletin* 60:581
- Wang JF, Feng JK, Ren AM, Liu XD, Ma YG, Lu P, Zhang HX (2004) *Macromolecules* 37:3451
- Becke AD (1993) *J Chem Phys* 98:5648
- Stephens PJ, Devlin FJ, Chabalowski CF, Frisch MJ (1994) *J Phys Chem* 98:11623
- Perdew JP, Wang Y (1992) *Phys Rev B* 45:13244
- Perdew JP (1991) In: Ziesche P, Eischrig H (eds) *Electronic structure of solids*. Akademie Verlag, Berlin
- Becke AD (1993) *J Chem Phys* 98:1372
- Ma J, Li SH, Jiang YS (2002) *Macromolecules* 35:1109
- Cao H, Ma J, Zhang GL, Jiang YS (2005) *Macromolecules* 38:1123
- Yang L, Feng JK, Ren AM, Sun JZ (2006) *Polymer* 47:1397
- Foresman JB, Head-Gordon M, Pople JA, Frisch MJ (1992) *J Phys Chem* 96:135
- Frisch MJ, Trucks GW, Schlegel HB, Scuseria GE, Robb MA, Cheeseman JR, Montgomery JA Jr, Vreven T, Kudin KN, Burant JC, Millam JM, Iyengar SS, Tomasi J, Barone V, Mennucci B, Cossi M, Scalmani G, Rega N, Petersson GA, Nakatsuji H, Hada M, Ehara M, Toyota K, Fukuda R, Hasegawa J, Ishida M, Nakajima T, Honda Y, Kitao O, Nakai H, Klene M, Li X, Knox JE, Hratchian HP, Cross JB, Bakken V, Adamo C, Jaramillo J, Gomperts R, Stratmann RE, Yazyev O, Austin AJ, Cammi R, Pomelli C, Ochterski JW, Ayala PY, Morokuma K, Voth GA, Salvador P, Dannenberg JJ, Zakrzewski VG, Dapprich S, Daniels AD, Strain MC, Farkas O, Malick DK, Rabuck AD, Raghavachari K, Foresman JB, Ortiz JV, Cui Q, Baboul AG, Clifford S, Cioslowski J, Stefanov BB, Liu G, Liashenko A, Piskorz P, Komaromi I, Martin RL, Fox DJ, Keith T, Al-Laham MA, Peng CY, Nanayakkara A, Challacombe M, Gill PMW, Johnson B, Chen W, Wong MW, Gonzalez C, Pople JA (2003) *Gaussian 03*, Revision B.04. Gaussian, Inc., Pittsburgh
- Brédas JL, Silbey R, Boudreaux DS, Chance RR (1983) *J Am Chem Soc* 105:6555
- Clarke TM, Gordon KC, Officer DL, Hall SB, Collis GE, Burrell AK (2003) *J Phys Chem A* 107:11505
- Pal B, Yen W-C, Yang JS, Chao CY, Hung YC, Lin ST, Chuang CH, Chen CW, Su W-F (2008) *Macromolecules* 41:6664
- Marcus RA, Sutin N (1985) *Biochim Biophys Acta* 811:265
- Nelsen SF, Trieber DA, Ismagilov RF, Teki Y (2001) *J Am Chem Soc* 123:5684
- Nelsen SF, Blomgren F (2001) *J Org Chem* 66:6551
- Ran X-Q, Feng J-K, Ren A-M, Li W-C, Zou L-Y, Sun C-Ch (2009) *J Phys Chem A* 113:7933